Journal of Magnetism and Magnetic Materials 322 (2010) 2360–2368

Contents lists available at ScienceDirect

Journal of Magnetism and Magnetic Materials

journal homepage: www.elsevier.com/locate/jmmm

Particle size effects on $La_{0.7}Ca_{0.3}MnO_3$: size-induced changes of magnetic phase transition order and magnetocaloric study

Wei Tang [a], Wenjian Lu [a,c,*], Xuan Luo [a], Bosen Wang [a], Xuebin Zhu [a], Wenhai Song [a], Zhaorong Yang [a], Yuping Sun [a,b,*]

[a] Key Laboratory of Materials Physics, Institute of Solid State Physics, Chinese Academy of Sciences, Hefei 230031, People's Republic of China
[b] High Magnetic Field Laboratory, Chinese Academy of Sciences, Hefei 230031, People's Republic of China
[c] Center for Strongly Correlated Materials Research, Department of Physics and Astronomy, Seoul National University, Seoul 151-742, Republic of Korea

ARTICLE INFO

Article history:
Received 6 December 2009
Received in revised form
12 February 2010
Available online 20 February 2010

Keywords:
Particle size
Magnetocaloric
Nanoparticle

ABSTRACT

The structure, magnetic properties, and magnetocaloric effect of $La_{0.7}Ca_{0.3}MnO_3$ ceramics with different particle sizes have been investigated. It is found that the Curie temperature increases first, and then decreases as particle size decreases and the type of magnetic phase transition changes from first-order to second-order, which may be attributed to surface pressure effects. The maximum magnetic entropy change $-\Delta S_M^{max}$ and relative cooling power (RCP) show non-monotonic behaviors with decreasing the particle size. However, for the 3400 nm sample, the magnetic entropy change $-\Delta S_M$ reaches the maximum values of 6.41 and 8.63 J/kg K for the field changes of 2.0 and 4.5 T, respectively. Furthermore, the estimated large RCP values under lower magnetic fields in $La_{0.7}Ca_{0.3}MnO_3$ are comparable with those of typical magnetic refrigerant materials in the corresponding temperature range, suggesting those compounds might be promising candidates for magnetic refrigeration.

1. Introduction

Magnetic refrigeration, based on the magnetocaloric effect (MCE), has received increasing attention as an alternative to the well-established compression–evaporation cycle for room-temperature applications [1]. Since the discovery of the giant MCE in $Gd_5(Si_xGe_{1-x})_4$ intermetallics [2], several other materials have been found to exhibit large MCEs, such as $La(Fe_{1-x}Si_x)_{13}$ alloys and their hydrides $La(Fe_{1-x}Si_x)_{13}H_y$, $MnFeP_xAs_{1-x}$ alloys and $Ni_{2-x}Mn_{1-x}Ga$ Heusler alloys [3–9]. However, these promising materials have several disadvantages such as large thermal and/or field hysteresis and expensive production cost, which are not beneficial for the actual magnetic refrigerant applications. So, it is desirable to seek after other magnetic refrigerant materials with not only large MCE but also several advantages such as high refrigerant capability, innocuity, low-cost production and room temperature.

In the past few decades, large MCE of perovskite manganites has been investigated experimentally and theoretically and their potential applications are the broad working temperature ranges due to easy controlling of the Curie temperature by doping routes [10,11]. Generally, the large magnetic entropy change of perovskite manganites mainly originates from the variation of the double exchange (DE) interaction of the Mn^{3+} and Mn^{4+} ions [12]. In addition, the strong spin-lattice coupling also plays an important role [13,14]. Previous reports have indicated that the properties of perovskite manganites at nanoscale are quite different from those at microscale [15,16]. As the particle size reduces to nanoscale, the manganites exhibit a number of special characters compared with their corresponding bulk materials, such as super-paramagnetism, surface spin-glass, large coercivities, low saturation magnetization and low-field magnetoresistance effect [17–20]. Recently, investigations have indicated that the particle downsize plays an obvious role in determination of the magnetic entropy change [21]. However, up to now, not much systematic work about the effects of particle size on MCE of $La_{1-x}A_xMnO_3$ (A, alkaline earth ion) has been reported.

In this work, $La_{0.7}Ca_{0.3}MnO_3$ ceramics with different particle sizes were prepared. The main objective is to investigate the variations of structure, magnetic properties and MCE as a function of particle size, which may be helpful to understand the MCE of nanoscale magnetic refrigerant materials.

2. Experimental details

Powder samples of $La_{0.7}Ca_{0.3}MnO_3$ were synthesized by the sol–gel technology with stoichiometric amounts of high-purity

* Corresponding authors at: Key Laboratory of Materials Physics, Institute of Solid State Physics, Chinese Academy of Sciences, Hefei 230031, People's Republic of China. Tel.: +0086 551 559 2757; fax: +0086 551 559 1434.
E-mail addresses: wjlu@issp.ac.cn (W.J. Lu), ypsun@issp.ac.cn (Y.P. Sun).

0304-8853/$ - see front matter © 2010 Elsevier B.V. All rights reserved.
doi:10.1016/j.jmmm.2010.02.038

La_2O_3, $CaCO_3$ and $Mn(NO_3)_2$ as starting reagents. The precursors were dissolved in nitric acid resulting in a transparent solution. Suitable amounts of citric acid and polyethylene glycol were added into the reactor and then mixed thoroughly. A complete homogenous brown gel was achieved after heating at 373 K and later it was decomposed by heating at 573 K for 10 h, during which a brown-black powder was formed; then was separated into several parts and annealed at different temperatures from 923 to 1673 K for 20 h to obtain black powder. The sintering with different temperatures and time can lead particles to grow in different sizes. In the sol–gel technique, the polyethylene glycol helps in forming a network of cations from the precursor solution, enabling phase formation at relatively low temperatures.

The phases of the powder samples were identified by X-ray diffraction (XRD) with Cu Kα radiation (Philips X'pert Pro). The structural parameters were obtained by fitting the experimental data of XRD using the standard Rietveld technique. The surface morphology of samples was studied by field-emission scanning electronic microscopy (FE-SEM). The magnetization measurements were carried out by using a Quantum Design superconducting quantum interference device (SQUID) ($1.8 \le T \le 400$ K, $0 \le H \le 5.0$ T) in the temperature range of 5–380 K. The specific heat measurements were performed in a commercial physical properties measurements system (PPMS) ($1.8 \le T \le 400$ K, $0 \le H \le 9.0$ T).

3. Results and discussions

3.1. Structural characterization

Fig. 1(a) shows XRD patterns of $La_{0.7}Ca_{0.3}MnO_3$ (LCMO) samples. It is found that all the samples are single-phase with an orthorhombic perovskite crystalline structure. Fig. 1(b) shows the zoom of the (200) peak in the diffraction patterns. Obviously, the central positions shift to high angles first and then low angles with increase in sintering temperatures, indicating the changes of the lattice parameters. The sizes of the particles are confirmed by SEM micrographs for all the samples. As shown in Fig. 2(a)–(f), the average particle size is estimated to be from 30 to 6600 nm corresponding to the annealing temperature from 923 to 1673 K.

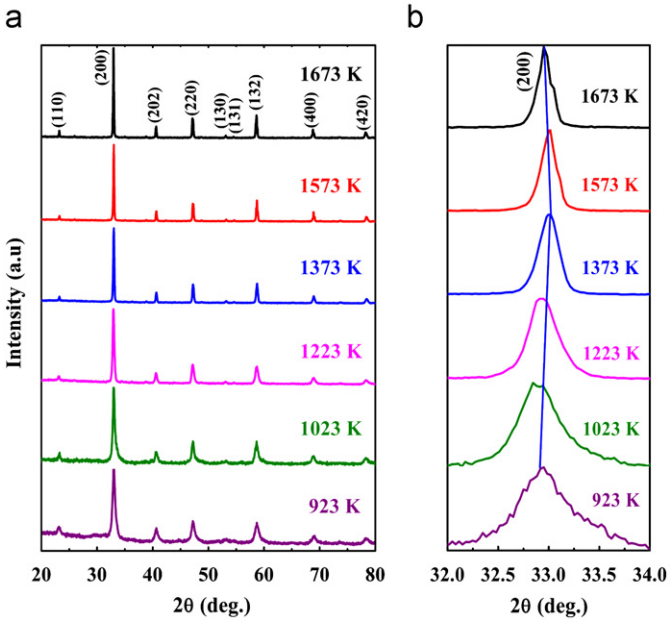

Fig. 1. (a) Room-temperature XRD patterns of LCMO particles annealed at different temperatures and (b) the zoom of the (200) peak in the diffraction patterns.

The full profile fitting to the room-temperature XRD spectrum for sample at 1673 K is shown in Fig. 3. The results from the Rietveld analysis are presented in Table 1. As shown in Fig. 4, the lattice parameters b, $c/2^{1/2}$ and V non-monotonously change with the variation of particle sizes. It also can be seen that the bond length $d_{Mn-O(1)}$ first decreases and reaches a minimum of 1.953 Å for the 160 nm sample, then increases and the $d_{Mn-O(2)}$ monotonously changes as particle size decreases, while the Mn–O–Mn bond angle has little change, indicating that the orthogonal lattice distortion changes with decrease in particle size [22] (Table 2).

3.2. Magnetic properties

Fig. 5 shows the temperature dependence of magnetization $M(T)$ for all samples measured at an applied magnetic field of 0.01 T in the zero-field cooling (ZFC), field-cooling cooling (FCC) and field-cooling warming (FCW) processes. The M–T data suggest that all these compounds undergo a paramagnetic (PM) to ferromagnetic (FM) transition upon cooling. In Fig. 5(a), an interesting feature is found that the ZFC magnetization at low temperature shows a gradual decline with the reduction of particle size. Furthermore, for the samples with 30 and 55 nm, the slopes of the ZFC curves are much larger than other samples about below 150 K, indicating the potentially magnetically disordered phase of the glass type. The magnetization decreases with the reduction of particle size due to the loss of long range FM order and the large local magnetic disorder on surface in the smaller-sized samples [23]. The abrupt decrease of magnetizations indicate that large MCE may exist around the magnetic transitions. In the inset of Fig. 5(b), the FCC and FCW curves of the samples with 6600, 3400 and 950 nm exhibit a very small thermal hysteresis, < 2 K, around T_C. The small thermal hysteresis is the aspiration of an engineer in applying MCE materials in a refrigerator. These features guarantee that the MCE is nearly reversible on temperature.

Fig. 6 shows the variation of Curie temperature T_C as a function of the particle size. The T_C is defined as the valley of dM/dT in the $M(T)$ curves. It is found that the T_C increases first and then tends to decrease with decrease in the particle size [24,25]. According to the DE theory, T_C is closely related to the magnitude of the oxygen 2p-like bandwidth $W_{O_{2p}}$. The bandwidth $W_{O_{2p}}$, depending on both bond angles and bond lengths, is described by [26]

$$W_{O_{2p}} \propto \cos\left[\tfrac{1}{2}(\pi-\theta_{Mn-O-Mn})\right]/d_{Mn-O}^{3.5}, \quad (1)$$

where $\theta_{Mn-O-Mn}$ is the Mn–O–Mn bond angle and d_{Mn-O} is the Mn–O bond length. As shown in Fig. 6, the calculated $W_{O_{2p}}$ values and the T_C almost show the same variation tendency with particle size, which suggests that the T_C variation may be attributed to the change of bandwidth. As shown in Fig. 7(a), the isotherm magnetization $M(H)$ curves of LCMO are plotted at 5 K with a maximum magnetic field of 4.5 T. Obviously, the magnetization increases sharply at low fields and then tends to be saturated above 1.0 T. Fig. 7(b) shows the magnetic moment M_S at 4.5 T and the coercivity H_C for all samples. It can be seen that the M_S per Mn ion reduces from 3.8 to 0.97 μ_B/f.u. with decrease in particle size, which may be related to the random canting of the particle surface spins caused by the competition between FM and antiferromagnetic exchange interactions near the surface [27]. In addition, the H_C declines as the particle size rises, indicating a gradual change from single domain to multidomain magnetic behavior with increase in the particle size [28].

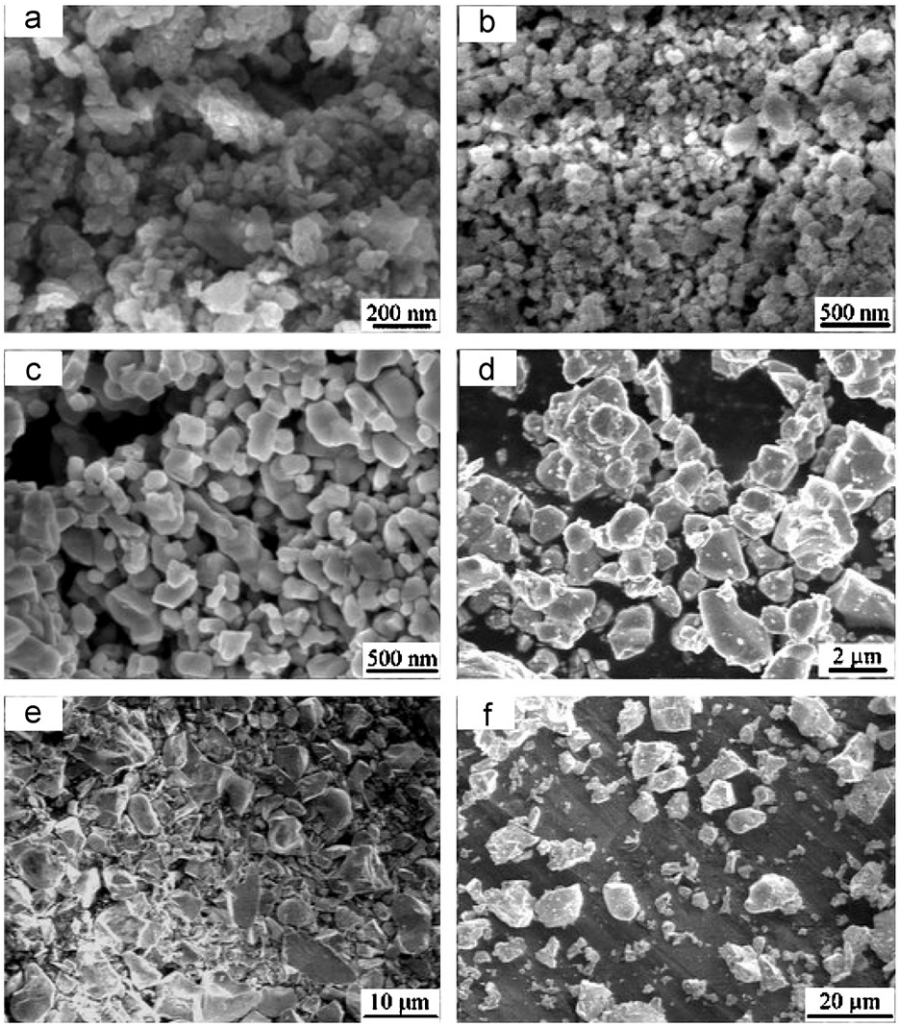

Fig. 2. Scanning electron micrographs of LCMO sintered at (a) 923 K, (b) 1023 K, (c) 1223 K, (d) 1373 K, (e) 1573 K and (f) 1673 K.

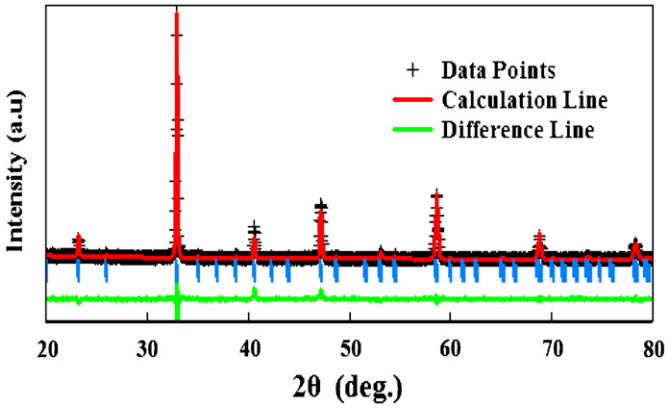

Fig. 3. Full profile fitting of XRD spectrum for sample at 1673 K.

Table 1
Lattice parameters of LCMO samples based on Rietveld refinement in the orthorhombic space group Pbnm of XRD patterns measured at room temperature.

Parameters	923 K	1023 K	1223 K	1373 K	1573 K	1673 K
d_{Mn-Mn} (Å)	3.859	3.859	3.867	3.867	3.868	3.865
$d_{Mn-O(1)}$ (Å)	1.967	1.965	1.953	1.955	1.956	1.959
$d_{Mn-O(2)}$ (Å)	1.959	1.959	1.964	1.964	1.964	1.967
	1.959	1.959	1.961	1.962	1.962	1.965
Mn–O(1)–Mn (deg.)	161.0	160.9	160.8	160.9	160.9	160.9
Mn–O(2)–Mn (deg.)	160.1	160.1	160.2	160.2	160.2	160.2
R_p (%)	5.61	6.91	8.13	5.85	6.45	8.69

In order to get a deeper insight of the type of magnetic transition, $M(H)$ curves are obtained around T_C in 2 K step as shown in Fig. 8. The corresponding Arrott plots (H/M vs M^2) from $M(H)$ curves are also obtained in Fig. 9. According to Banerjee's criterion, a negative or a positive sign of the slope of H/M vs M^2 curves in the critical region corresponds to the first- or second-order magnetic phase transition, respectively [29]. Fig. 9(a)–(c) indicate the samples with 6600, 3400 and 950 nm exhibit a first-order magnetic phase transition due to the negative slope at high field region. However, in Fig. 9(d)–(f), no obvious negative slopes are observed, indicating a second-order transition for these samples.

Previous investigations have confirmed that the surface pressure acts on the particles due to the decrease in the size [30]. Usually, the induced surface pressure may change the type of magnetic phase transition. So, the observed change from first-order to second-order magnetic phase transition in present samples could be attributed to the effects of the particle size reduction. Moreover, it is reported that the T_C firstly increases at low pressure and then decreases with increasing pressure further

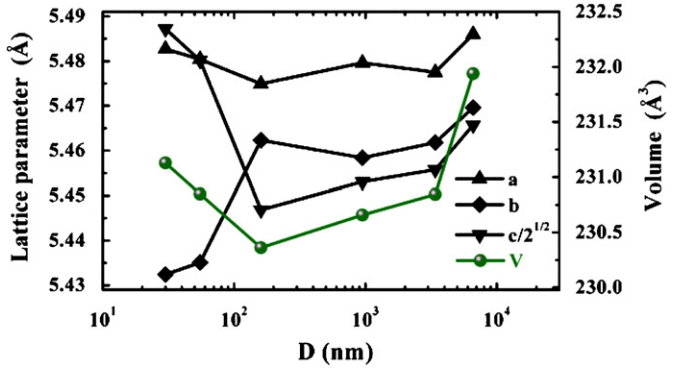

Fig. 4. The variations of the lattice parameters a, b, $c/2^{1/2}$, and the unit-cell volume V with particle size.

Table 2
Sintering temperature T_S, average particle size D, Curie temperature T_C, magnetic moment M_S at 4.5 T, and coercivity H_C.

T_S (K)	D (nm)	T_C (K)	M_S (μ_B/f.u.)	H_C (T)
1673	6600	235	3.59	0.0030
1573	3400	260	3.61	0.0043
1373	950	268	3.81	0.0072
1223	160	270	3.33	0.0167
1023	55	263	1.92	0.0267
923	30	236	0.97	0.0474

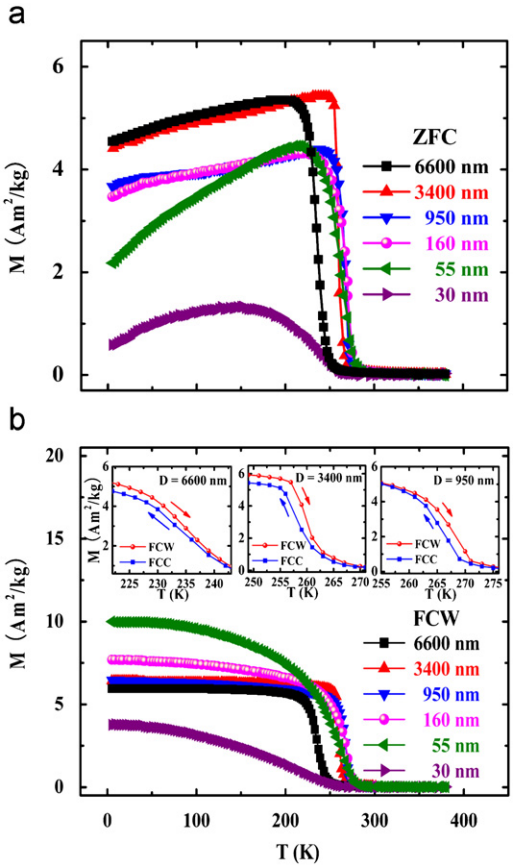

Fig. 5. (a) Temperature dependence of magnetization recorded in the ZFC and (b) FCW modes under an applied magnetic field H=0.01 T. The inset shows the FCC and FCW curves of the samples with 6600, 3400, and 950 nm.

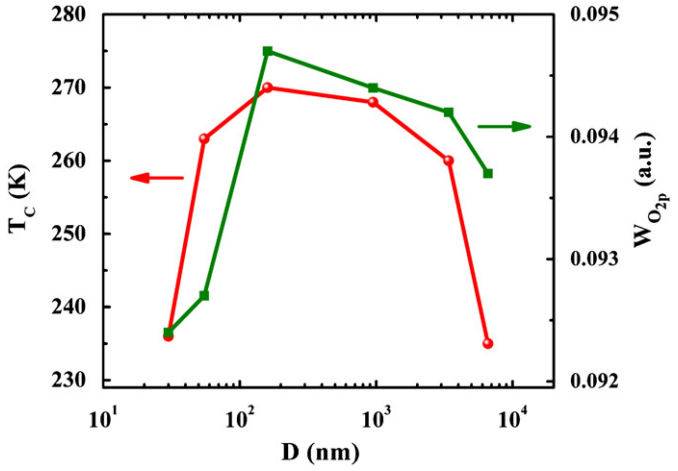

Fig. 6. Curie temperature T_C and bandwidth $W_{O_{2p}}$ with the variation of particle size.

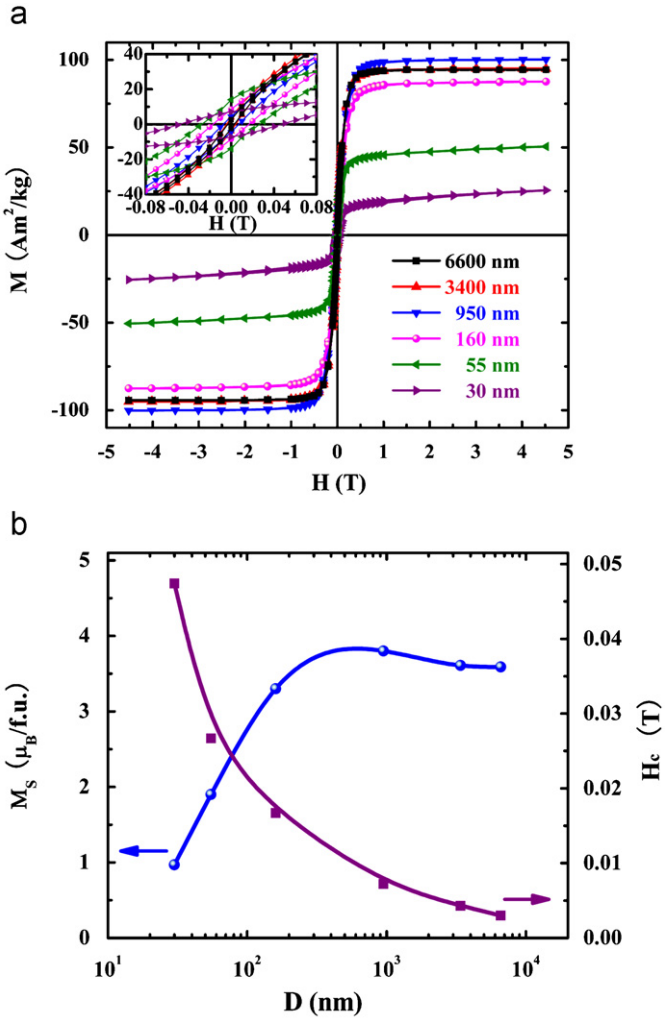

Fig. 7. (a) Isotherm magnetization curves $M(H)$ at 5 K for samples with different particle sizes and (b) the magnetic moment M_S at 4.5 T and coercivity H_C. The inset shows the isotherm magnetization curves in the low field region.

and the Curie–pressure curve reaches a broad peak for pressure close to 4 GPa [31]. So, the maximum value of T_C corresponding to the 160 nm sample indicates that the surface pressure for this sample should be close to 4 GPa. For further reduction of the

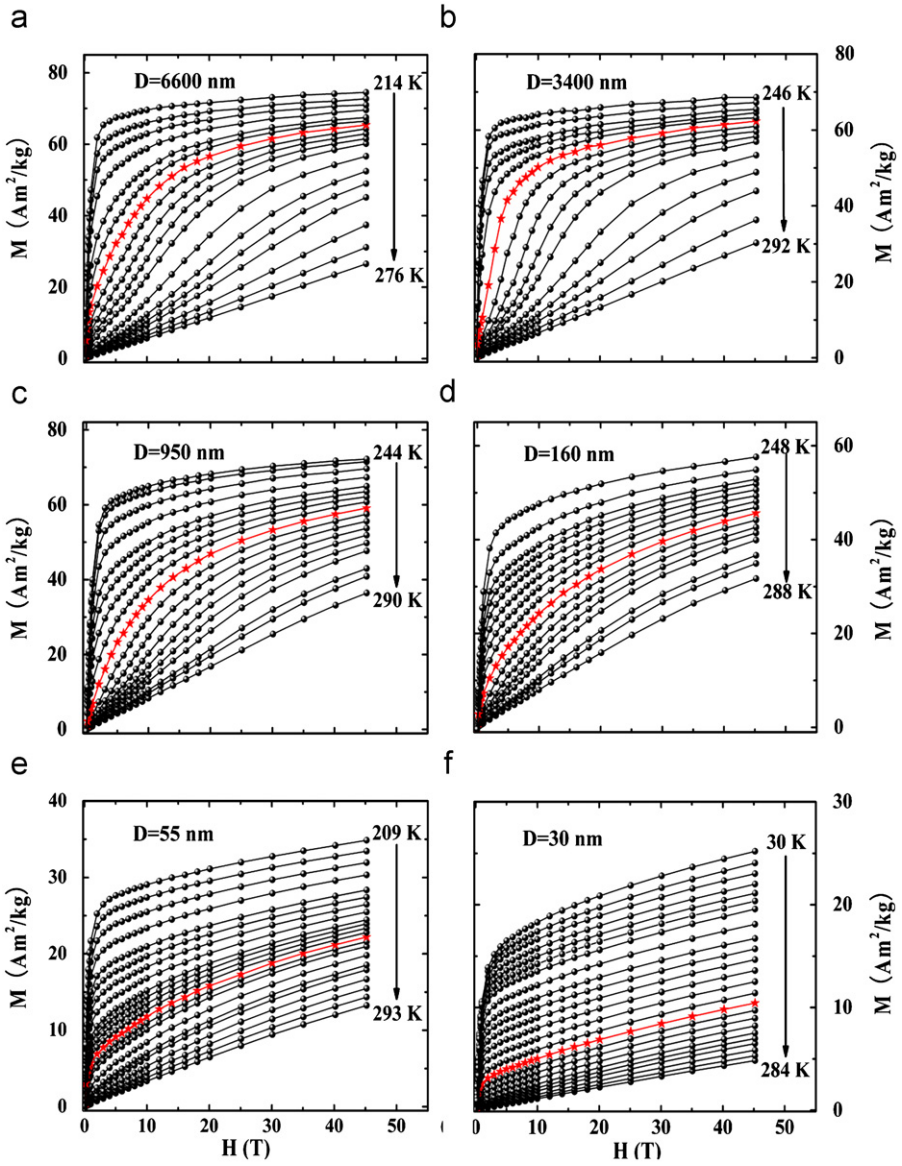

Fig. 8. Initial magnetization isotherms $M(H)$ for all samples at different temperatures around T_C. The red line is magnetic transition temperature (T_C) (For interpretation of the references to colour in this figure legend, the reader is referred to the web version of this article.).

particle size, the Jahn–Teller distortion will be enhanced, resulting in the decrease of T_C. Based on the analysis, the relationship between the particle size and the magnetic properties could be well understood. As the particle size decreases, at first, the induced surface pressure will compact the lattice, which may result in the reduction of the cell volume and the broadening of the bandwidth leading to the enhancement of T_C as the previous reports about external pressure effects; with further reduction of particle size, the Jahn–Teller distortion are gradually enhanced leading to the expansion of cell volume and the decrease of T_C.

3.3. Magnetocaloric properties

From the classical thermo-dynamical theory, the magnetic entropy change $-\Delta S_M$ induced by the variation of a magnetic field from H_1 to H_2 can be evaluated by the measurement of $M(H)$ curves [32–34]:

$$\Delta S_M(T,\Delta H) = S_M(T,H_2) - S_M(T,H_1) = \int_{H_1}^{H_2} \left(\frac{\partial S}{\partial H}\right)_T dH \quad (2)$$

according to a thermodynamic Maxwell's relation,

$$\Delta S_M(T,\Delta H) = \int_{H_1}^{H_2} \left(\frac{\partial M}{\partial T}\right)_H dH. \quad (3)$$

For a first-order transition, there is a singularity in the equation mentioned above and the discontinuous magnetic entropy change around the transition should be taken into account [35].

From Eq. (3), $-\Delta S_M$ associated with the magnetic field and/or temperature variation has been calculated from the measured $M(H)$ curves shown in Fig. 8. As shown in Fig. 10, the temperature dependence of $-\Delta S_M$ are plotted as a function of temperature with different magnetic field changes of ΔH=0.5–4.5 T. As expected from Eq. (3), the peak of $-\Delta S_M$ may occur around T_C where the variation in magnetization as a function of temperature is the sharpest. The maximum magnetic entropy changes $-\Delta S_M^{max}$ and related data are summarized in Table 3. Obviously, the values of $-\Delta S_M^{max}$ for 6600 and 950 nm samples are close to each other, but the T_C of the two samples are much different, indicating the values of T_C and $-\Delta S_M^{max}$ can be well adjusted by changing the

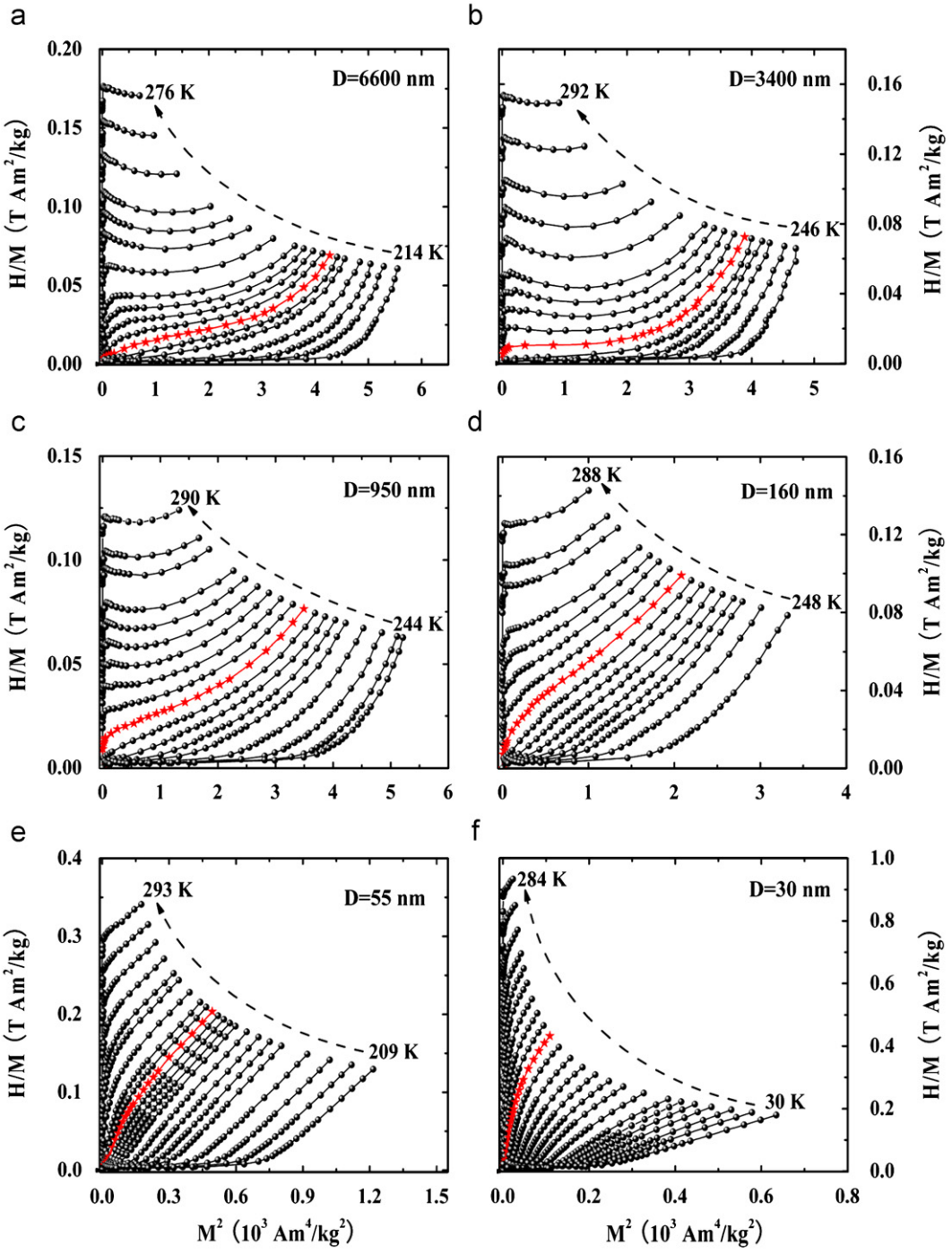

Fig. 9. Arrott plots (H/M vs. M^2). The red line is magnetic transition temperature (T_C) (For interpretation of the references to colour in this figure legend, the reader is referred to the web version of this article.).

particle sizes. Moreover, as shown in Fig. 11(a), the peak of the temperature dependence of $-\Delta S_M$ broadens with decrease in particle size. This is because of the gentle decrease in magnetization close to the FM–PM transition of the continuous second-order phase transitions. The $-\Delta S_M^{max}$ for the field changes $\Delta H=0.5$, 1.0, 2.0, 3.0 and 4.5 T are about 3.30, 4.73, 6.41, 7.46 and 8.63 J/kg K, respectively. Especially for 2.0 T, the $-\Delta S_M^{max}$ of LCMO reaches 6.4 J/kg K, which is much larger than that for Gd (4.2 J/kg K, $\Delta H=2.0$ T) [1]. Another important parameter for a MCE material is adiabatic temperature change ΔT_{ad}. Based on thermodynamics, an approximate estimation of ΔT_{ad} at an arbitrary temperature T has been performed from the measured $-\Delta S_M$ using the expression [36]

$$\Delta T_{ad} \cong -\frac{T}{C_P}\Delta S_M(T,H) \tag{4}$$

where C_P is the zero-field specific heat. The data are not show here. Fig. 12 shows the temperature dependence of ΔT_{ad} with different particle sizes for the applied magnetic field changes up to 2.0 and 4.5 T. It is observed that ΔT_{ad} almost maintains the nature of $-\Delta S_M$. The maximum peak values of ΔT_{ad} are about 3.09 and 4.30 K for field changes of 2.0 and 4.5 T, respectively.

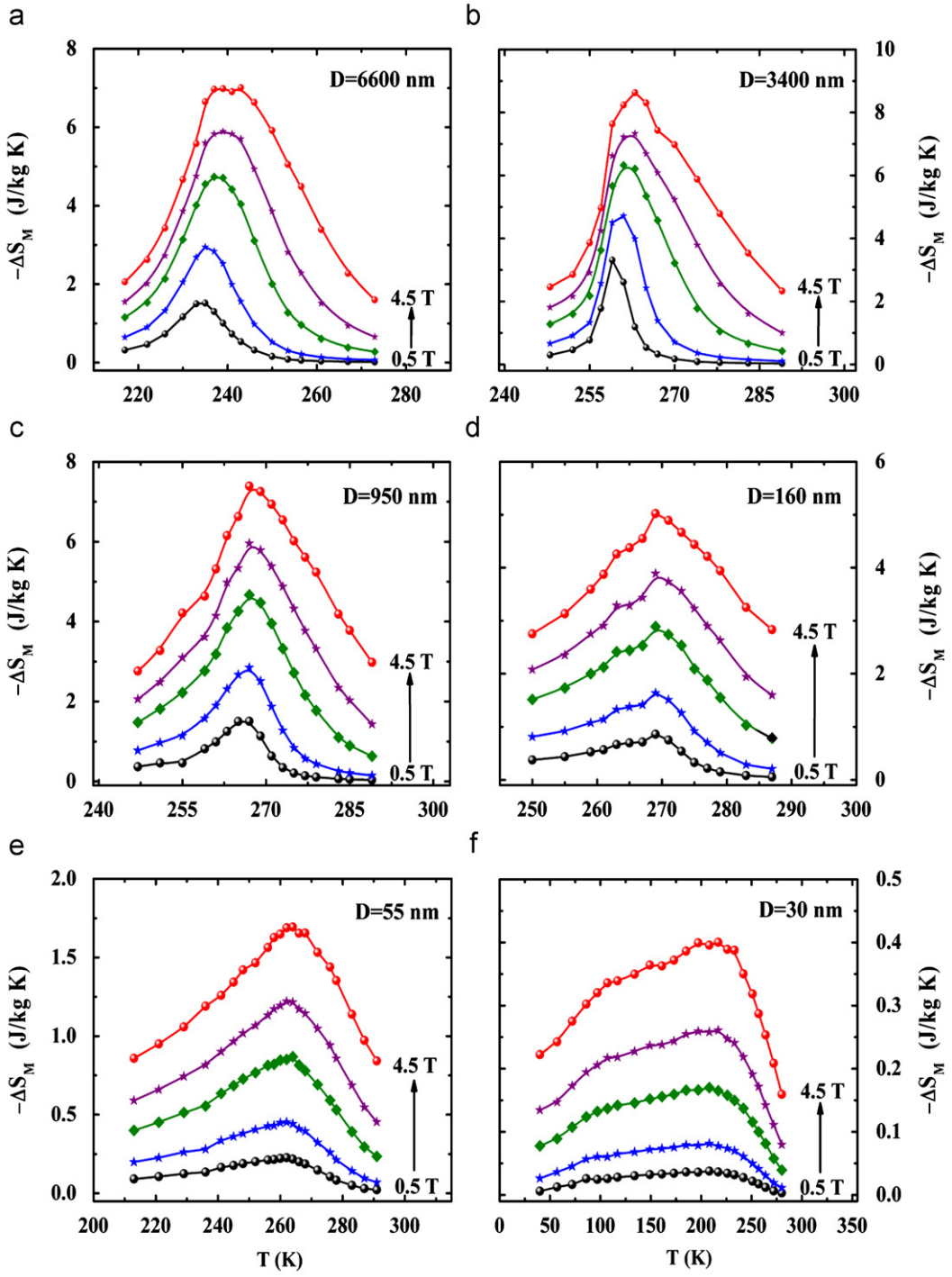

Fig. 10. Temperature dependence of magnetic entropy change and $-\Delta S_M$ under $\Delta H = 0.5$, 1.0, 2.0, 3.0, and 4.5 T.

In the framework of the mean field theory, the relation between $-\Delta S_M^{\max}$ and the magnetic field near T_C is given as [37]

$$\Delta S_M^{\max} = -1.07qR\left(\frac{g\mu_B JH}{kT_C}\right)^{2/3}, \quad (5)$$

where q is the number of magnetic ions, R is the gas constant and g is the Lande factor. The $H^{2/3}$ dependence of $-\Delta S_M^{\max}$ is depicted in Fig. 11(b). For the particle sizes below 160 nm, it can be seen clearly that $-\Delta S_M^{\max}$ is perfectly linearly dependent on $H^{2/3}$, indicating the second-order magnetic transition under the framework of the mean field theory [38], which is well consistent with the above results of magnetizations. Based on the above results, it can be concluded that the particle size can easily modulate the type of the phase transition in present compounds.

The magnetic cooling efficiency of a magnetocaloric material can be evaluated by considering the magnitude of $|\Delta S_M|$ and its full-width at half maximum (δT_{FWHM}) [10]. It is easy to establish the product of the $|\Delta S_M^{\max}|$ and the δT_{FWHM} as

$$RCP = |\Delta S_M^{\max}| \times \delta T_{FWHM}, \quad (6)$$

which stands for the so-called relative cooling power (RCP) as one of the most important parameters for selecting potential

Table 3
Maximum magnetic entropy change $-\Delta S_M^{max}$ and RCP of LCMO samples.

Samples ID (K)	D (nm)	$-\Delta S_M^{max}$ (J/kg K)					RCP (J/kg)				
		0.5 T	1.0 T	2.0 T	3.0 T	4.5 T	0.5 T	1.0 T	2.0 T	3.0 T	4.5 T
1673	6600	1.52	2.95	4.74	5.83	6.99	22.1	49.0	104.0	156.8	243.1
1573	3400	3.30	4.73	6.41	7.46	8.63	19.6	42.1	88.4	131.4	213.9
1373	950	1.51	2.85	4.67	5.96	7.39	18.3	43.3	96.0	156.6	241.6
1223	160	0.86	1.64	2.89	3.89	5.02	16.9	41.2	91.6	139.1	218.4
1023	55	0.23	0.45	0.87	1.22	1.69	11.0	26.0	56.6	85.5	134.6
923	30	0.04	0.08	0.17	0.26	0.40	6.6	15.7	36.1	61.2	103.2
Gd	–	1.70	2.80	4.20	7.10	–	–	–	–	–	–

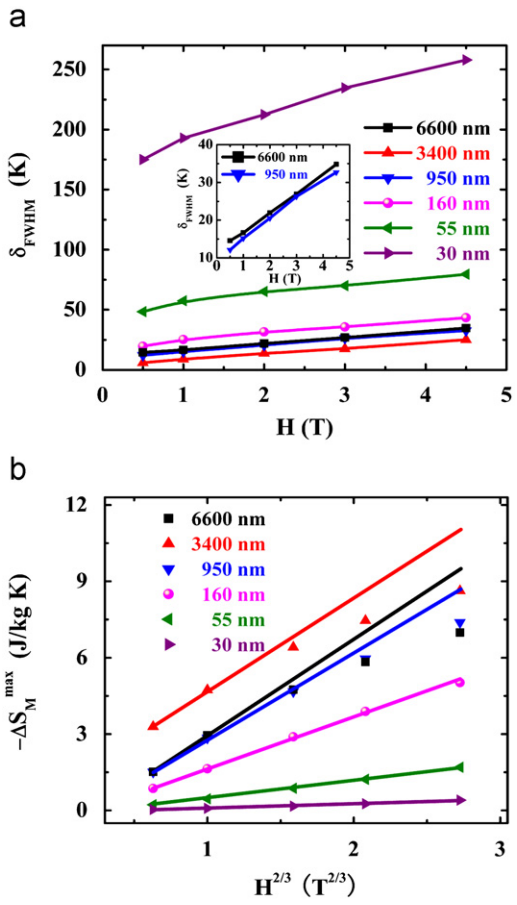

Fig. 11. (a) Full-width at half maximum δT_{FWHM} of $-\Delta S_M$ peak for LCMO as a function of magnetic field H and (b) maximum magnetic entropy change $-\Delta S_M^{max}$ as a function of $H^{2/3}$.

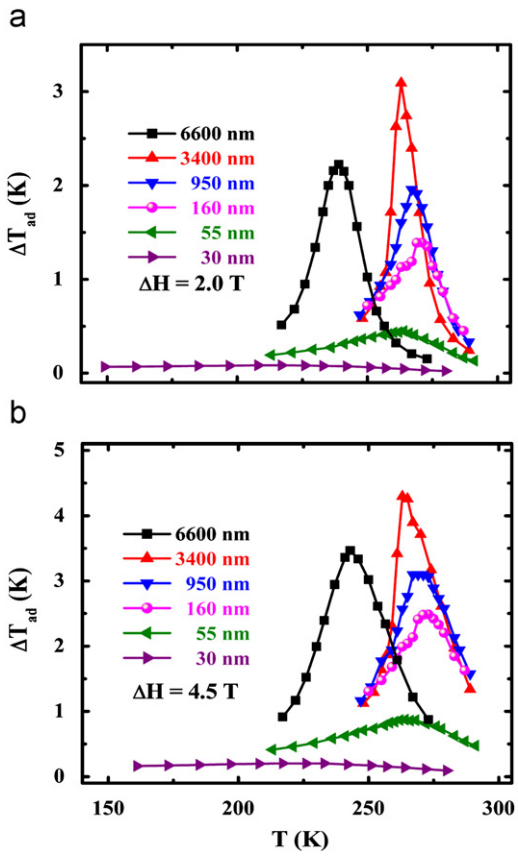

Fig. 12. Temperature dependence of ΔT_{ad} with different particle sizes for the magnetic field changes up to 2.0 and 4.5 T.

substances for magnetic refrigerants. Fig. 13 shows the particle size dependence of RCP for all samples at different magnetic fields. Obviously, the values of RCP gradually increase with increasing magnetic fields. It is found that the maximum value of the RCP is about 243 J/kg for a field change of 4.5 T. In particular, a large value of RCP is obtained to be 104 J/kg for a relatively low field change of 2.0 T. For comparison, the values of RCP for some representative magnetic refrigerant materials and our studied systems with a field change of 2.0 T are plotted in Fig. 14 [39–41]. The RCP values of LCMO with different particle sizes are much larger than that of $Ni_{55.5}Mn_{20}Ga_{24.5}$. For the 6600 nm sample, the RCP value is close to that of $MnAs_{0.75}Sb_{0.25}$ and is about 61% of Gd with a field change of 2.0 T. Furthermore, considering the advantages of perovskite manganites, such as high efficiency, good chemical stability, tunable ordering temperature by doping methods, higher electrical resistivity and low production costs, suggests those compounds could be more promising candidates for magnetic refrigeration.

4. Conclusions

In summary, the structure, magnetic properties and magnetocaloric effect of $La_{0.7}Ca_{0.3}MnO_3$ ceramics were studied. It is found that the type of magnetic phase transition changes from first-order to second-order with decrease in the particle size. However, the T_C changes non-monotonically as a function of particle size, which can be attributed to the competition between surface pressure effect and Jahn–Teller distortion effect. The $-\Delta S_M^{max}$ are about 6.41 and 8.63 J/kg K at 2.0 and 4.5 T, respectively.

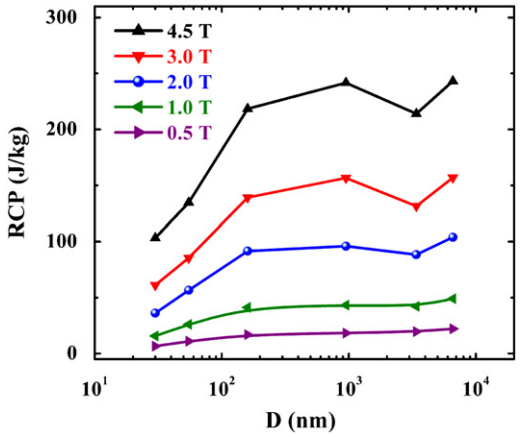

Fig. 13. The particle size dependence of RCP for all samples under different applied fields.

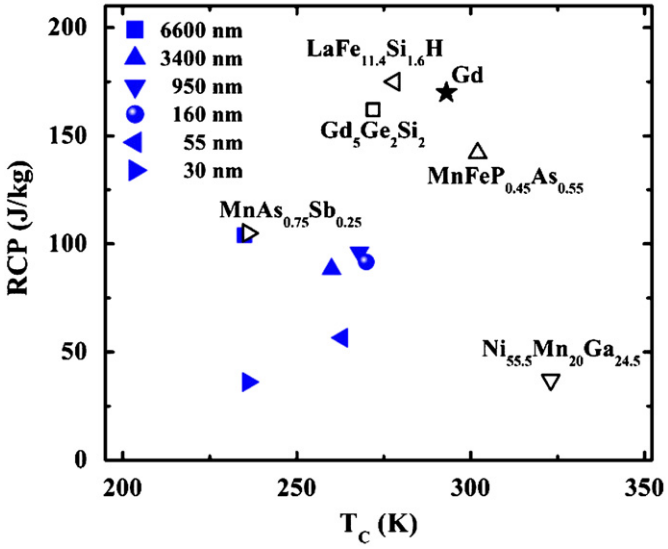

Fig. 14. The comparison of RCP values of LCMO with those of potential candidates for magnetic refrigeration ($\Delta H = 2.0$ T).

Furthermore, the RCP values at low field are well comparable with the commercial magnetic refrigerant materials, indicating that the $La_{0.7}Ca_{0.3}MnO_3$ ceramics could be considered as good candidates for magnetic refrigeration.

Acknowledgements

This work was supported by the National Key Basic Research under Contract No. 2007CB925002 and the National Nature Science Foundation of China under Contract Nos. 10804111, 10774146, 50672099 and 50701042 and Director's Fund of Hefei Institutes of Physical Science, Chinese Academy of Sciences.

References

[1] Y. Dan'kov, A.M. Tishin, V.K. Pecharsky, K.A. Gschneidner Jr., Phys. Rev. B 57 (1998) 3478.
[2] V.K. Pecharsky, K.A. Gschneidner Jr., Phys. Rev. Lett. 78 (1997) 4494.
[3] F.X. Hu, B.G. Shen, J.R. Sun, Z.H. Cheng, G.H. Rao, X.X. Zhang, Appl. Phys. Lett. 78 (2001) 3675.
[4] A. Fujita, S. Fujieda, Y. Hasegawa, K. Fukamichi, Phys. Rev. B 67 (2003) 104416.
[5] O. Tegus, E. Brück, K.H.J. Buschow, F.R. de Boer, Nature 415 (2002) 150.
[6] E. Brück, M. Llyn, A.M. Tishin, O. Tegus, J. Magn. Magn. Mater. 290 (2005) 8.
[7] F. Albertini, F. Canepa, S. Cirafici, E.A. Franceschi, M. Napoletano, A. Paoluzi, L. Pareti, M. Solzi, J. Magn. Magn. Mater. 272 (2004) 2111.
[8] M. Pasquale, C.P. Sasso, L.H. Lewis, J. Appl. Phys. 95 (2004) 6918.
[9] X.Z. Zhou, W. Li, H.P. Kunkel, G. Williams, J. Phys.: Condens. Matter 16 (2004) L39.
[10] M.H. Phan, S.C. Yu, J. Magn. Magn. Mater. 308 (2007) 325.
[11] K.A. Gschneidner Jr., V.K. Pecharsky, Int. J. Refrig. 31 (2008) 945.
[12] M.H. Phan, S.C. Yu, N.H. Hur, J. Magn. Magn. Mater. 262 (2003) 407.
[13] Z.B. Guo, Y.M. Du, J.S. Zhu, H. Huang, W.P. Ding, D. Feng, Phys. Rev. Lett. 78 (1997) 1142.
[14] S.L. Yuan, Z.C. Xia, L. Liu, W. Chen, L.F. Zhao, J. Tang, G.H. Zhang, L.J. Zhang, H. Cao, W. Feng, Y. Tian, L.Y. Niu, S. Liu, Phys. Rev. B 68 (2003) 184423.
[15] F. Chen, H.W. Liu, K.F. Wang, H. Yu, S. Dong, X.Y. Chen, X.P. Jiang, Z.F. Ren, J.M. Liu, J. Phys.: Condens. Matter 17 (2005) L467.
[16] P. Katiyar, D. Kumar, T.K. Nath, A.V. Kvit, J. Narayan, S. Chattopadhyay, W.M. Gilmore, S. Coleman, C.B. Lee, J. Sankar, Appl. Phys. Lett. 79 (2001) 1327.
[17] R.D. Sánchez, J. Rivas, C. Vázquez-Vázquez, A. López-Quintela, M.T. Causa, M. Tovar, S. Oseroff, Appl. Phys. Lett. 68 (1996) 134.
[18] R. Mahesh, R. Mahendiran, A.K. Raychaudhuri, C.R. Rao, Appl. Phys. Lett. 68 (1996) 2291.
[19] A.K.M. Akther Hossain, L.F. Cohen, F. Damay, A. Berenov, J. MacManus-Driscoll, N.McN. Alford, N.D. Mathur, M.G. Blamire, J.E. Evetts, J. Magn. Magn. Mater. 192 (1999) 263.
[20] P.K. Siwach, H.K. Singh, O.N. Srivastava, J. Phys.: Condens. Matter 20 (2008) 273201.
[21] V. Provenzano, A.J. Shapiro, R.D. Shull, Nature 429 (2004) 853.
[22] T. Zhang, G. Li, T. Qian, J.F. Qu, X.Q. Xiang, X.G. Li, J. Appl. Phys. 100 (2006) 094324.
[23] R.N. Bhowmik, A. Poddar, R. Ranganathan, C. Mazumdar, J. Appl. Phys. 105 (2009) 113909.
[24] W.J. Lu, X. Luo, C.Y. Hao, W.H. Song, Y.P. Sun, J. Appl. Phys. 104 (2008) 113908.
[25] L.E. Hueso, J. Rivas, F. Rivadulla, M.A. López-Quintela, J. Appl. Phys. 86 (1999) 3881.
[26] Y. Tokura, in: Colossal Magnetoresistive Oxides, Gordon and Breach, London, 2000.
[27] E.L. Nagaev, Phys. Rep. 346 (2001) 387.
[28] C.N. Chinnasamy, B. Jeyadevan, K. Shinoda, K. Tohji, D.J. Djayaprawira, M. Takahashi, R.J. Joseyphus, A. Narayanasamy, Appl. Phys. Lett. 83 (2003) 2862.
[29] S.K. Banerjee, Phys. Lett. 12 (1964) 16.
[30] T. Sarkar, P.K. Mukhopadhyay, A.K. Raychaudhuri, S. Banerjee, J. Appl. Phys. 101 (2007) 124307.
[31] C.W. Cui, T.A. Tyson, Z. Zhong, J.P. Carlo, Y.H. Qin, Phys. Rev. B 67 (2003) 104107.
[32] T. Hashimoto, T. Numasawa, M. Shino, T. Okada, Cryogenics 21 (1981) 647.
[33] V.K. Pecharsky, K.A. Gschneidner Jr., J. Appl. Phys. 86 (1999) 565.
[34] V.K. Pecharsky, K.A. Gschneidner Jr., A.O. Pecharsky, A.M. Tishin, Phys. Rev. B 64 (2001) 144406.
[35] N.A. de Oliveira, P.J. von Ranke, Phys. Rev. B 77 (2008) 214439.
[36] V.K. Pecharsky, K.A. Gschneidner Jr., J. Magn. Magn. Mater. 200 (1999) 44.
[37] V. Franco, J.S. Blázquez, A. Conde, Appl. Phys. Lett. 89 (2006) 222512.
[38] H. Oesterreicher, F.T. Parker, J. Appl. Phys. 55 (1984) 4336.
[39] E. Brück, J. Phys. D: Appl. Phys. 38 (2005) R381.
[40] K.A. Gschneidner Jr., V.K. Pecharsky, J. Appl. Phys. 93 (2003) 4722.
[41] H. Wada, T. Morikawa, K. Taniguchi, T. Shibata, Y. Yamada, Y. Akishige, Physica B 328 (2003) 114.